Available online at www.sciencedirect.com
ScienceDirect
Journal of Catalysis 255 (2008) 234–240
JOURNAL OF CATALYSIS
www.elsevier.com/locate/jcat

Dual pulsed-beam controlled mole fraction studies of the catalytic oxidation of CO on supported Pd nanocatalysts

C.J. Harding *, S. Kunz, V. Habibpour, V. Teslenko, M. Arenz, U. Heiz

Lehrstuhl für Physikalische Chemie, Technische Universität München, D-85747 Garching, Germany

Received 30 November 2007; revised 18 January 2008; accepted 15 February 2008

Available online 17 March 2008

Abstract

The characterisation of nanocatalytic materials was performed by pulsed molecular beam studies. Dual piezo-controlled pulsed molecular beams were used to probe oxidation reactions through their ability to accurately control the mole fraction of reactants. By varying the size of mass-selected Pd clusters soft-landed onto thin MgO films, strong dependency of the cluster size in the catalytic oxidation of CO was observed. True size effects were clearly observed only when experimental results were compensated for in the incoming flux. This correction led to determination of the reaction probability, the most unambiguous method of characterisation. Strong parallels between the new results for small, mass-selected clusters and grown, mass-distributed clusters can be clearly seen.

Keywords: Nanocatalysis; Palladium; Mass-selected; Clusters; p-MBRS; Mole fraction; Oxidation; CO

1. Introduction

Catalytic CO oxidation on Pd is one the most well-studied reactions. Many of the major experiments were carried out by Ertl et al. on Pd single crystals, leading to important discoveries, such as the observation that CO oxidation follows a Langmuir–Hinshelwood mechanism [1,2]. Other important aspects of catalytic oxidation have been illustrated by experiments on subsurface oxygen, which was shown to induce kinetic oscillations under the specific conditions required for CO oxidation [3].

Driven by the possible industrial application of this work, developments in the field have led to investigations of dispersed metal particles on chemically inert supports, due to the financial benefits associated with scaled-up versions of the catalytic material involving less precious metals. The important question then arises: Is there any chemical difference between Pd particles on support materials compared with a single crystal? For Pd particles in the nanometer size regime, which have small interparticle distances compared with the particle diameters, experimental measurements can be well interpreted assuming single-crystal properties. Examples of such observations include CO poisoning which inhibits oxygen adsorption and consequently affects the reaction kinetics [4–6]; even kinetic oscillations have been observed for Pd islands supported by oxide films [7]. However, the catalytical properties of smaller Pd clusters (up to ∼100 atoms) on metal-oxide supports have not been fully established.

Knowledge of the origin and functionality of nanocatalysts of smaller mass-selected and larger mass-distributed clusters is an ever-growing field of scientific interest. The catalytic properties of atomic clusters and larger mass-distributed nanoparticles have been investigated with respect to support interactions [8–17] and size-dependent electronic and chemical properties [11,18–20]. In the characterisation of these catalysts, spectroscopic techniques such as IR [13,21–23] and electron spectroscopy [24–26] have revealed interesting aspects of the nanocatalysts. In many catalytic studies, size effects have been shown to play a dominant role in the effectiveness of the catalyst; however the dynamic aspects of catalytically activated reactions are often well illustrated by molecular beam measurements. Many such experiments have been performed on mass-distributed nanoparticles [5,7,9,27–29], but fewer have

* Corresponding author.
E-mail address: christopher.harding@mytum.de (C.J. Harding).

0021-9517/$ – see front matter
doi:10.1016/j.jcat.2008.02.008

been carried out on smaller, size-selected cluster-based catalysts [30,31].

Mass selection in the production of supported catalysts allows creation of clusters consisting of exact numbers of atoms, allowing superior control when describing size effects in catalysis. Probing these smaller mass-selected clusters with molecular beam techniques can unlock fundamentally interesting details about the reaction path if the molecular beams can be precisely controlled. If the mole fraction of the reactants can be determined, then reactant-rich and -poor regimes can be investigated. Mole fraction isotherms and trends in cluster size variation are then augmented by this additional information. When the contribution of reverse spillover [32,33] is determined in such experiments [31], further crucial details may be elucidated. The reverse spillover contributions can be calculated using the capture zone model [29]. The formalism involves determining a global sticking probability that allows separation of the product flux into direct and indirect reactant flux.

In short, the capture zone model is a kinetic model used to incorporate the flow of reactants from a support material to the active centres (in this case, Pd clusters). A concentration profile is calculated between neighbouring clusters, called the capture zone. Any reactant molecules lying on the support within this capture zone will reach the cluster and react. As such, the capture zone acts as a slow reservoir of reactants. The model assumes an equivalent frequency factor for the adsorption and desorption processes, resulting in a dependency on the saddle energy (i.e., the energetic difference between adsorption and diffusion) and the adsorption site spacing, both of which are constant values [29]. In addition, the model relies on the assumptions that the sticking probability of CO on Pd is unity and that of CO on the support also remains unaffected by other physical parameters. Due to the former assumption in the capture zone model, explicit reference to the CO sticking probability is omitted from any formalism that follows. The reverse spillover of oxygen is neglected due to the very low adsorption energy of molecular oxygen on MgO films [34]. Using this model, the reaction probability (RP) can be determined.

When discussing the effects of particle size in catalysis, the RP is the only relevant quantity. It gives the statistical chance of reaction on the catalyst and as such provides the best available description of cluster-based materials. Whereas the turnover frequency negates the influence of reactant flux, the RP does not. When a factor as important as the incoming molecule rate is overlooked, very different and possibly fallacious conclusions may be drawn from the experimental data.

Here we present experimental data investigating temperature and size effects of small (up to Pd_{30}) clusters by considering effects induced by the variation of the reactant mole fractions. This work offers an important extension of our previous work [29], because for the first time we were able to control and change the mole fraction of the reactants on size-selected clusters supported on a thin oxide film. Using the capture zone model, the experimental data may be further resolved into RPs, the *de facto* quantity in the characterisation of a supported catalyst. The importance of RPs in the interpretation of size effects for small clusters is clearly illustrated.

2. Experimental

Nanocatalysts are produced by the soft-landing of size-selected Pd clusters onto a MgO substrate. The support is prepared by evaporating magnesium in an isotropic oxygen background and allowing it to grow onto a cleaned Mo(100) crystal surface (Mg evaporation rate, 1–2 ML min^{-1}; O_2 background, 5×10^{-7} mbar). The films have a typical thickness of ∼10 ML. Before the deposition of clusters onto the support, the MgO film was annealed to 800 K [35,36]. Auger electron spectroscopy was used to ensure the quality and cleanliness of the support.

The Pd clusters were produced using a 100 Hz laser vaporisation source [20], in which the third harmonic of a Nd:YAG laser is focused onto a rotating Pd target. The metal plasma produced was combined with a helium carrier gas, and the thermal mixture was pulsed through a piezo-controlled nozzle, creating a supersonic expansion. The positively charged metal clusters were allowed to traverse a set of ion optics until they reached a mass-selecting quadrupole (ABB-Extrel; mass limit, 4000 amu). The mass gate of the quadrupole was programmed to select only masses of a given value and allow their deposition onto the MgO film. The mass-selected, charged Pd clusters were deposited at 90 K (to prevent agglomeration) up to a desired coverage. The coverage was chosen based on the cluster size, to provide an identical catalytically active surface area on the support (assuming spherical cluster structures) as achieved experimentally through integration of the cluster current. This contrasts with other methods in which the cluster size and coverage cannot be controlled independently. For Pd_n ($n = 8, 13, 30$) the required cluster coverages were 0.65% ML, 0.47% ML and 0.28% ML respectively, where 1 ML = 2.25×10^{15} clusters cm^{-2} deposited onto a 0.8-cm^2 crystal. The cluster charge was neutralised on impact with the MgO film, either by defect neutralisation or through charge-tunnelling interactions with the thin film.

After formation of the supported catalyst, double pulsed-beam measurements were conducted to investigate the effects of the mole fraction variation of the product gases. The pulsed-beam assembly and its operation have been described in detail previously [30,31]. In addition to previous studies, the experiment was extended to include a second pulsed molecular beam, which allows controlled variation of the mole fraction. The reaction of interest was the oxidation of carbon monoxide to form carbon dioxide. The product molecules were detected and the mole fractions of the pulsed beams were calibrated using a Balzers QMG 421 quadrupole mass spectrometer. The entrance of the mass spectrometer is covered by a skimmer that was biased by −150 V, to prevent electron-stimulated desorption processes [37] and mounted in the line of sight of the catalyst. The signal from the detector of the mass spectrometer (90° SEV) is passed into a preamplifier (Balzers EP 112) before it is averaged (15–20 pulses; pulse frequency, 0.3 Hz; pulse duration, 100 ms) and read by a digital oscilloscope (LeCroy Waverunner 6030).

The mole fraction of the reactant gases was controlled by the calibrated ion current value. This value was achieved by collecting the mass channel that corresponds to a reactant and then

controlling the back-pressure of the reactant gas. The height of the first reactant channel was then set to a height at the proper ratio with that of the second reactant channel. The maximum height for the spectrometer output was defined to ensure that the detector did not become saturated at any point during the measurement. In all of the subsequent measurements, the two molecular beams were pulsed simultaneously onto the catalytic surface. The two molecular beams were aligned to be coincident with the sample. The total gas flux remained constant.

The temperature of the reaction was controlled by resistive heating of the crystal. The temperature feedback system was controlled by software designed in-house (Labview).

3. Results

3.1. Catalytic characterisation

Signals recorded using the data acquisition procedure were analysed to extract quantitative values that allow a thorough characterization of nanocatalytic materials. The raw data in the form of quadrupole mass spectrometry (QMS) response were analysed with respect to the peak maximum. The peak maximum persists for 30 ms, during which the system is assumed to be in pseudo-steady state, as shown in Fig. 1. The value for the peak height was calculated from the average of the data over the steady-state regime. A typical flux value of 1×10^{16} cm^{-2} s^{-1} in this regime corresponds to an effective gas pressure of 3.5×10^{-5} mbar at the surface. Error determination was based on statistical deviations within the pseudo-steady-state region of the recorded data. The error in the peak height was calculated from the standard deviation of the points over this time period. The error for the mole fraction value was calculated by considering the average steady-state value of the reactants and given as a percentage of the stated mole fraction value.

The flux of CO onto the surface, as measured by the QMS detector, can be resolved into total, direct, and indirect components using the capture zone model. First, the incoming CO rate (F_{CO}) is normalised to the area of the surface ($A = 0.8$ cm^{-2}) to calculate the amount of incoming CO every second per unit area of the surface (the flux). The total incoming flux ($J_{tot,CO}$) onto a cluster then can be described through the global sticking probability (α_g), calculated using the capture zone formalism,

$$J_{tot,CO}\left(\text{CO s}^{-1}\,\text{cm}^{-2}\right) = \frac{\alpha_g}{A} F_{CO}. \tag{1}$$

The direct flux ($J_{dir,CO}$) of the reactant (assuming a cluster-sphere model) CO onto a single cluster is defined by

$$J_{dir,CO}\left(\text{CO s}^{-1}\,\text{cm}^{-2}\right) = \left(\frac{R}{A}\right)^2 \pi F_{CO}, \tag{2}$$

where R is the radius of the cluster. Because the total reactant flux is simply the sum of the direct and indirect fluxes ($J_{diff,CO}$) of CO onto the clusters ($J_{tot,CO} = J_{diff,CO} + J_{dir,CO}$), the diffusing flux of CO onto a cluster can be calculated from

$$\begin{aligned} J_{diff,CO}\left(\text{CO s}^{-1}\,\text{cm}^{-2}\right) &= J_{tot,CO} - J_{dir,CO} \\ &= \left(\frac{\alpha_g}{A} - \frac{\pi R^2}{A^2}\right) F_{CO}. \end{aligned} \tag{3}$$

Once the incoming flux has been resolved into its two constituent parts, the RP for the two reactant channels can be calculated. First, however, the product reactant flux must be determined. As described previously, the pseudo-steady-state method was adopted, allowing the product rate of CO_2 (F_{CO_2}) to be determined from the measured QMS response. The flux can then be used to calculate the turnover frequency (TOF) of the catalyst. The TOF effectively indicates the efficiency of the catalyst, giving the rate of CO_2 produced for every cluster on the surface; it is calculated by

$$\text{TOF}\left(\text{CO}_2\,\text{s}^{-1}\,\text{cm}^{-2}\,\text{n}^{-1}\right) = \frac{1}{nA} F_{CO_2}, \tag{4}$$

where n is the number of atoms, clusters, or normalisation to the area of the catalyst. From the standard definition of enzyme catalysis,[1] n is the number of active sites of the catalyst; however, the number of active sites is ambiguous in heterogeneous catalysis and is difficult to quantify. Consequently, for the remainder of this paper, the TOF is calculated with respect to the number of clusters present. For clarity, TOF values for different definitions of n are given in Table 1. Normalising the TOF to the total, direct, or indirect flux of CO, the RP for the overall, direct, or indirect flux channels can be obtained from

$$\text{RP} = \frac{F_{CO_2}}{F_{inc}}, \tag{5}$$

a unitless quantity simply describing the likelihood of reactivity on a catalyst, where F_{inc} is the generic form of the incoming flux. For all RP values in the following, the reactant flux was normalised by the total incoming flux of CO.

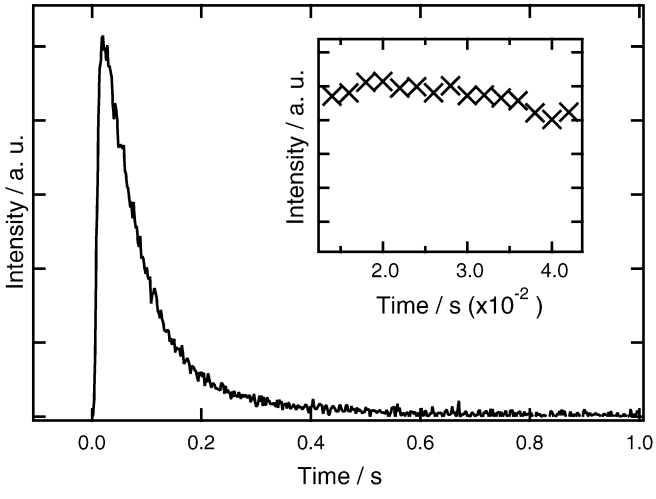

Fig. 1. Shown is the response of the mass spectrometer on detection of the CO_2 reaction products. Inset is the peak of the signal on a different scale illustrating the pseudo steady-state regime.

[1] IUPAC Compendium of Chemical Terminology, 2nd edition, 1997.

Table 1
Turn over frequency (TOF) values for various clusters sizes at a given mole fraction and temperature value illustrating the TOF magnitude according to the various definitions possible

	Cluster size		
	Pd_8[a]	Pd_{13}[b]	Pd_{30}[c]
TOF per cluster	14.4	36.2	33.1
TOF per atoms	1.8	2.8	1.1
TOF per effective area	4.8×10^{15}	8.8×10^{15}	4.6×10^{15}

[a] $x_{CO} = 0.5$; cluster coverage 0.65% ML; temperature 478 K.
[b] $x_{CO} = 0.5$; cluster coverage 0.47% ML; temperature 478 K.
[c] $x_{CO} = 0.5$; cluster coverage 0.28% ML; temperature 478 K.

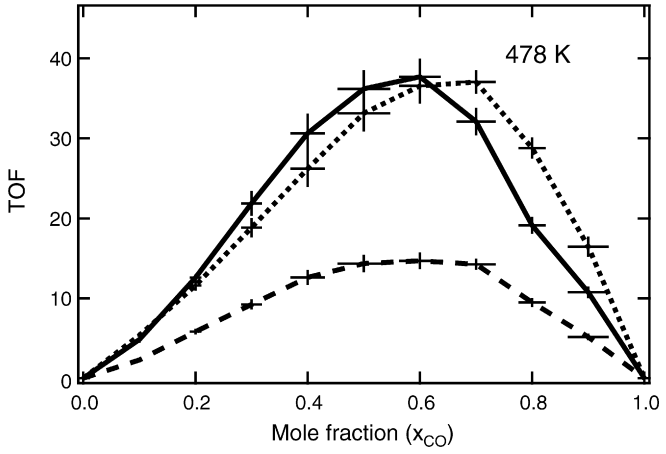

Fig. 2. The turn over frequency (TOF) is shown for three different cluster sizes at a varying CO mole fraction. (- - -) indicates TOFs determined using a catalyst based on mass-selected Pd_8, (—) using Pd_{13} and (· · ·) using Pd_{30}. The constant temperature at which the kinetics were determined was 478 K. The coverage of each cluster size is given in the text. The size of the marker illustrates the error in the measurements.

3.2. TOF

The rate of CO_2 production, per cluster (TOF) was calculated for a varying mole fraction as a function of cluster size (Fig. 2). TOFs for the investigated cluster sizes were recorded at a constant temperature of 478 K, an arbitrary value selected to ensure catalytic activity. A very striking dependency with variations in cluster size can be seen, in which the CO_2 production rate of the Pd_{13}- and Pd_{30}-based catalysts was almost twice that of the Pd_8-based catalyst. As the TOF was normalised to the number of clusters, CO_2 production would be expected to increase with increasing cluster size. At mole fractions of zero or unity, the CO_2 production is zero regardless of the clusters on the surface, due to the lack of CO and O_2 reactants, respectively. For a given cluster size (at a fixed temperature), CO_2 production increased from zero (at $x_{CO} = 0$) to a maximum, before decreasing again to zero (at $x_{CO} = 1$). The observed dependency of the production rate on the mole fraction may be rationalised by considering the adsorption properties of the reactants.

At low mole fractions of CO (i.e., CO-poor regime), the rate-determining step was likely the adsorption of CO; consequently, CO_2 production was low. As the mole fraction of CO approached unity, the rate-determining step then became the dissociative adsorption of O_2, and once again the rate of CO oxidation was low.[2] Thus, CO_2 production would be expected to be the maximum at a value between these two extremes, as was observed. It can be seen that at a given temperature, the maximum CO_2 production was achieved for all cluster sizes with a mole fraction of ∼0.6 within the defined error limits (although the nominal maximum for Pd_{30} was at a mole fraction of ∼0.7). This value is the expected stoichiometric ratio (2:1) for the CO oxidation reaction. The decreased rate of the CO_2 production away from this (optimum) mole fraction value was more rapid under CO-rich conditions due to a reversible site-blocking mechanism. Consequently, due to the presence of adsorbed CO, the dissociative adsorption of O_2 became less efficient when the adsorption sites were hindered by the adsorption of CO, and thus the rate decreased faster under CO-rich conditions.

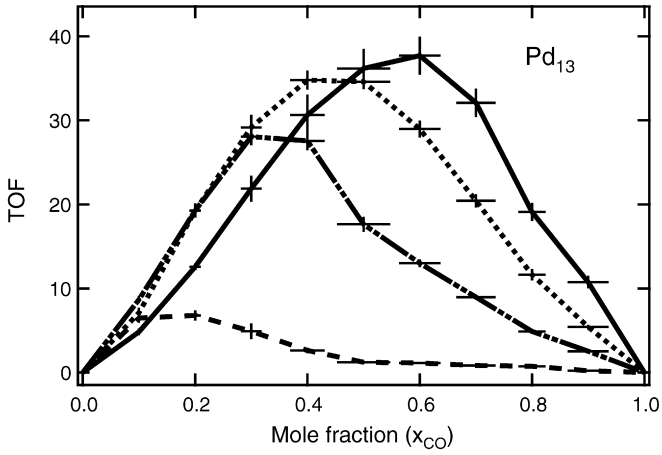

Fig. 3. The turn over frequency (TOF) is shown for a catalyst based on mass-selected Pd_{13} at a constant coverage of 0.47% ML. The mole fraction dependent TOFs were recorded at four different temperatures. The TOFs at different temperatures are illustrated with (- - -, 358 K), (– · · – · ·, 417 K), (· · ·, 440 K) and (—, 478 K) lines. The size of the marker illustrates the error in the measurements.

The variation of CO_2 production with temperature for a given cluster size was investigated for Pd_{13} mass-selected clusters with a coverage of 0.47% ML. The mole fraction measurements for a range of four different temperatures are given in Fig. 3. In the CO-poor regime (at low mole fraction values), the rate was proportional to the CO flux. Only at the highest temperature was a slight variation in this behaviour seen. Under CO-rich conditions, as noted earlier, the rate-determining step became the dissociative adsorption of O_2. In parallel with expectations for a temperature-activated process, as the temperature increased, CO_2 production also increased. Furthermore, the mole fraction of the maximum production also shifted toward higher temperatures. This shift can be attributed to reversible site-blocking effects that have been reported for larger metallic particles [7]. At lower temperatures, CO site blocking was enhanced due to an increased magnitude of the sticking proba-

[2] We assume for the CO oxidation, a Langmuir–Hinshelwood mechanism, involving the dissociative adsorption of O_2.

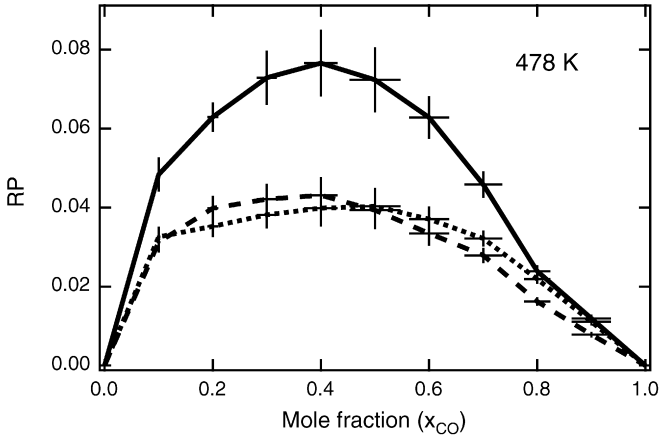

Fig. 4. The reaction probability (RP) is shown for three different cluster sizes at varying CO mole fraction. (- - -) indicates RPs determined using a catalyst based on mass-selected Pd_8, (—) using Pd_{13} and (· · ·) using Pd_{30}. The constant temperature at which the kinetics were determined was 478 K. The coverage of each cluster size is given in the text. The size of the marker illustrates the error in the measurements.

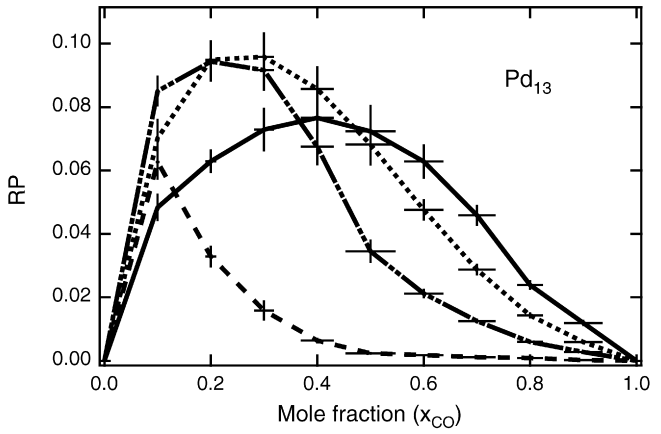

Fig. 5. The reaction probability (RP) is shown for a catalyst based on mass-selected Pd_{13} at a constant coverage of 0.47% ML. The mole fraction dependent RPs were recorded at four different temperatures. The RP values at different temperatures are illustrated with (- - -, 358 K), (– · · – · ·, 417 K), (· · ·, 440 K) and (—, 478 K) lines. The size of the marker illustrates the error in the measurements.

bility. In addition, the dissociation of O_2 was reduced at lower temperatures.

3.3. Reaction probabilities

The TOF measurements can be further refined by considering the RP. The data in Figs. 2 and 3 can be normalised to the flux of the incoming CO corrected by the capture zone model, as described previously. Fig. 4 shows the variation of RP with cluster size corrected for the total flux (including both diffusion and direct flux). The RP varied in the same way as the TOF across the range of mole fractions investigated, except that the maximum values were closer to a mole fraction of ∼0.4. One interesting feature seen when comparing the RP and the TOF is that in the case of Pd_{30} and Pd_8, the probability was approximately the same (∼4%), but much lower than that when Pd_{13} was used (∼8%). At a first glance, this appears to be in direct contradiction to the TOF data (Fig. 2), but rather than showing an anomalous result, it highlights the importance of the use of RPs in conjunction with TOFs to demonstrate the clear and very significant size effects. It should be noted that these results appear to contrast with previous work [31], but in the case of the earlier measurements, the clusters were precovered with oxygen, making them essentially incomparable with those used in the present study.

Finally, when considering the temperature effects for Pd_{13} clusters, we found similar results (Fig. 5) as for the TOF measurements (Fig. 3). The maximum RP value shifted to a higher mole fraction with increasing temperature; furthermore, the maximum overall RP was achieved at an intermediate temperature of 440 K. However, maximum CO_2 formation occurred at higher mole fraction values when TOFs were considered compared with RPs.

Under CO-poor conditions, the RP appeared to be independent of temperature. At low CO mole fractions, the rate-determining step depends on the availability of CO adsorption sites. At higher mole fractions, the reaction depends on temperature activation. As the temperature is increased, the CO sticking probability decreases (O_2 dissociation increases), occupation of reactive sites by CO decreases, and, consequently, CO_2 formation increases. However, a different behaviour was observed at the highest temperature (478 K). At higher temperatures, the assumptions made in the model—specifically, that the CO sticking probability on Pd is equal to unity—became invalid, and the model began to break down.

4. Discussion

With control over the mole fraction, the observed trends in the experimental data demonstrate that the maximum production of CO_2 occurred close to the stoichiometric ratio. At lower mole fraction values, the catalyst was precovered with O_2, and thus CO_2 production was governed by the CO flux. At higher mole fractions, the converse occurred. Therefore, optimum conditions were reached when the catalyst was covered with the stoichiometric ratio of reactants. This finding is in good agreement with previous results on Pd nanoparticles and clearly indicates that supported size-selected Pd clusters serve as model catalytic systems.

The first apparent discrepancy between the conclusions drawn from considering TOF and RP for the same system is that when the RP is considered, the mole fraction at which the maximum CO_2 production occurs moves away from the ideal. When the RP is evaluated, the resulting values no longer contain information about the reaction stoichiometry, because the values are normalised only to the CO flux; consequently, the maximum probability occurs at a different (lower) mole fraction value. These considerations also apply when formulating a definition for the RP [Eq. (5)].

When the size of the clusters is considered, catalytic CO_2 production appears to be greater for the Pd_{13} and Pd_{30} clusters. The results from catalysts based on these two larger cluster sizes demonstrate an evolution of CO_2 at a rate twice that for the Pd_8

clusters. When the incoming flux is taken into consideration, the RP values do not directly complement the conclusions drawn from the TOF data, because the cluster coverage is calculated to ensure that the effective coverage remains constant. It should be noted that in principle, the cluster coverage defines which reaction channel is predominant for the RP. In the case of direct flux, the RP is independent of the cluster coverage.

Previous work at the high CO mole fraction limit [31] has shown that reverse spillover coverage dependency is important for clusters of this size, especially in the case of Pd_{30}. It has been demonstrated that the RPs for CO defined in terms of direct and indirect fluxes (i.e., reverse spillover) are not necessarily equivalent. In addition, the behaviour of the different reservoirs of reactant molecules varies as a function of cluster size. Here, only the total flux to the clusters (a sum of the direct and indirect reaction channels) is considered, highlighting the effects of varying mole fraction. Calculating the RP in this way demonstrates that Pd_8 and Pd_{30} have identical probabilities for reaction. This suggests that Pd_8 and Pd_{30} are equally efficient catalysts under the current conditions [31], whereas Pd_{13} (with an RP twice that of Pd_8 and Pd_{30}) is much more efficient. However, based on the TOF values, the amount of CO_2 produced by Pd_{30} is equivalent to that of Pd_{13} and twice that of Pd_8. This illustrates the misleading nature of TOF measurements. Only when the total reactant flux is considered can Pd_{13} be clearly defined as the most effective catalyst.

Although the Pd_{30} clusters are larger, the surface area of the support material remains constant, implying that fewer Pd_{30} clusters are present on the surface. Thus, the Pd_{30} clusters are surrounded by much more free space compared with their smaller counterparts. The diffusion from the film onto the cluster is a very important factor in CO_2 production, as is the intercluster spacing.

Each cluster has an associated capture zone that acts as a CO reservoir. It is important to note that the capture zone model does not have a fixed capture zone radius, but rather it behaves as a function of the concentration profile between two neighbouring clusters. Note that it is the actual physical situation that is referred to in the interpretation that follows.

When the size of the cluster is large, so is the associated capture zone, but because there are relatively few clusters on the surface, dead space between the cluster capture zones is expected. In those regions, the CO remains on the film, but it is too far away from any cluster to ever react. Consequently, the RP is high, as is the TOF. As the cluster size decreases, the capture zone also decreases, but the number of clusters increases. In a mid-sized cluster regime, the capture zones are sufficiently close to reduce the dead space but sufficiently sparse so that the capture zones do not overlap. In this regime, both the TOF and RP are expected to be high and to not differ from the values seen with high amounts of dead space. The limiting case would be when the capture zones of the clusters touched. When the size is further decreased and the capture zones start to overlap, the TOF will start to decrease even though the RP may remain high.

As the clusters become smaller, the space between them reduces to such an extent that eventually the capture zones begin to overlap. At this point, even though the dead spaces are very small and in the overlapping regions, the CO molecules are shared between more than one cluster. This effectively reduces the efficiency of the catalysts, because the amount of CO reaching each active centre is attenuated by nearest-neighbour competition. Consequently, the TOF should decrease irrespective of the RP.

Because the measured TOFs for Pd_{13} and Pd_{30} are large compared with that for Pd_8, a strong influence from overlapping capture zones cannot be demonstrated. In principle, Pd_{30} should have the highest CO_2 production, with the TOF decreasing as the size decreases and the capture zones overlap. Thus, the effects of reverse spillover can be considered small in the spectra, but the effects of size are clarified and highlighted. The difference in CO_2 production is largely due to the electronic properties of the clusters. In addition, the Pd_{13} cluster appears to be the best for the oxidation of CO within the size range investigated.

If the cluster size is maintained but the temperature is varied, then additional effects are observed. First, as the temperature is increased, the maximum mole fraction in the TOF also increases. Again, this maximum is lower when the RP is considered, for the same reasons as discussed earlier.

For both the RP and TOF, the higher the CO_2 production in an increasingly CO-poor regime, the lower the temperature becomes. Occupation of adsorption sites by CO at lower temperatures may effectively lead to a reversible but strong active site occupation that is alleviated at higher temperatures. Such a mechanism also has been observed in larger particles [7]. For mass-distributed clusters in the nanometer size regime (∼2700 Pd atoms), stark and asymmetric decreases in the steady-state CO_2 production are seen at a mole fraction between 0.3 and 0.6 as the temperature is varied over a range of 70 K. The site-blocking effects for larger (6 nm) nanoparticles (and thus the asymmetry) are less than those for single crystals [9]. Consequently, as the size of the clusters is further reduced, so is the abrupt nature of this effect. For smaller clusters (∼100 Pd atoms), the asymmetric profile of the CO_2 production remains, but the abrupt decrease is less pronounced. Extending the size regime by considering smaller clusters (∼9 to 30 Pd atoms) should result in similar trends, as was observed. Such clear agreement between smaller and larger Pd clusters reinforces the need to consider a broad size distribution to completely understand cluster catalysis.

Despite the apparent temperature limitations of the reverse-spillover model, the maximum production of CO_2 nonetheless increased constantly with increasing temperature. However, these measurements cannot provide explicit details of the catalytic energy barrier that must be overcome to provide efficient CO_2 production.

5. Conclusion

Mole fraction measurements represent one of a very important set of measurements that allow investigation of the dynamics of nanocatalysts and characterization of such materials. Temperature effects, as well as strong size effects, are seen

for cluster-based catalytic materials involving Pd size-selected clusters deposited onto thin films of MgO. Small, mass-selected Pd clusters show similar active site blocking by adsorbate molecules as systems based on larger particles of the same metal. The calculation of reverse spillover, and thus the ability to normalise TOF data to the incoming flux, is also very important. In this way, the presence of slow reservoirs of CO and their contribution to the incoming flux may be taken into account. The resulting RP allows the correct interpretation of data by allowing the actual origin of the reactants to be deduced, thereby enabling unambiguous characterisation.

Our findings demonstrate that catalytic reactions are complex and depend strongly on particle size. These size effects must be considered in the design of catalytic materials. Although the TOF values provide an indispensable route to optimising the reaction conditions, true size effects can only be detected when the RP is calculated. This information can only be obtained when the particle size and coverage are controlled independently. The importance of control over the temperature and mole fraction should be considered in the search for the most effective and efficient way to catalyse reactions.

Acknowledgments

Financial support was provided by the Deutsche Forschungsgemeinschaft (DFG) and the European Union within the GSOMEN project and the COST D41 program. The authors thank Martin Röttgen for his work during the initial stages of this study.

References

[1] T. Engel, G. Ertl, J. Chem. Phys. 1267 (1978) 69.
[2] T. Engel, G. Ertl, Chem. Phys. Lett. 95 (1978) 54.
[3] S. Ladas, R. Imbihl, G. Ertl, Surf. Sci. 88 (1989) 219.
[4] J. Libuda, I. Meusel, J. Hoffmann, J. Hartmann, L. Piccolo, C.R. Henry, H.J. Freund, J. Chem. Phys. 4669 (2001) 114.
[5] I. Meusel, J. Hoffmann, J. Hartmann, J. Libuda, H.J. Freund, J. Phys. Chem. B 3567 (2001) 105.
[6] T. Engel, G. Ertl, The Chemical Physics of Solid Surfaces and Heterogeneous Catalysis, Elsevier, New York, 1982.
[7] V. Johanek, M. Laurin, A.W. Grant, B. Kasemo, C.R. Henry, J. Libuda, Science 1639 (2004) 304.
[8] C.R. Henry, Surf. Sci. Rep. 231 (1998) 31.
[9] J. Libuda, H.J. Freund, Surf. Sci. Rep. 157 (2005) 57.
[10] B. Yoon, H. Häkkinen, U. Landman, A.S. Wörz, J.-M. Antonietti, S. Abbet, K. Judai, U. Heiz, Science 403 (2005) 307.
[11] U. Heiz, E.L. Bullock, J. Mater. Chem. 564 (2004) 14.
[12] M. Arenz, U. Landman, U. Heiz, ChemPhysChem 1871 (2006) 7.
[13] A.S. Wörz, U. Heiz, F. Cinquini, G. Pacchioni, J. Phys. Chem. B 18418 (2005) 109.
[14] U. Landman, B. Yoon, C. Zhang, U. Heiz, M. Arenz, Top. Catal. 145 (2007) 44.
[15] J. Hagen, L.D. Socaciu, U. Heiz, T.M. Bernhardt, L. Wöste, Europ. Phys. J. D 327 (2003) 24.
[16] H. Häkkinen, W. Abbet, A. Sanchez, U. Heiz, U. Landman, Angew. Chem. Int. Ed. 1297 (2003) 42.
[17] A. Sanchez, S. Abbet, U. Heiz, W.D. Schneider, H. Häkkinen, R.N. Barnett, U. Landman, J. Phys. Chem. A 9573 (1999) 103.
[18] A. Kaldor, D.M. Cox, M.R. Zakin, in: I. Prigogine, S.A. Rice (Eds.), Molecular Surface Chemistry: Reactions of Gas-Phase Metal Clusters, Wiley, New York, 2007.
[19] W.D. Knight, K. Clemenger, W.A. de Heer, W.A. Saunders, M.Y. Chou, M.L. Cohen, Phys. Rev. Lett. 2141 (1984) 52.
[20] U. Heiz, W.D. Schneider, Crit. Rev. Solid State Mater. Sci. 251 (2001) 26.
[21] T. Schalow, B. Brandt, M. Laurin, S. Schauermann, S. Guimond, H. Kuhlenbeck, J. Libuda, H.J. Freund, Surf. Sci. 2528 (2006) 600.
[22] A.S. Wörz, K. Judai, S. Abbet, U. Heiz, J. Am. Chem. Soc. 7964 (2003) 125.
[23] K. Judai, S. Abbet, A.S. Wörz, U. Heiz, L. Giordano, G. Pacchiono, J. Phys. Chem. B 9377 (2003) 107.
[24] G. Ertl, J. Küppers, Low Energy Electrons and Surface Chemsitry, VCH, Weinheim, 1985.
[25] S. Krischok, J. Gunster, D.W. Goodman, O. Hofft, V. Kempter, Surf. Interface Anal. 77 (2005) 37.
[26] S. Krischok, P. Stracke, V. Kempter, Appl. Phys. A Mater. Sci. Proc. 167 (2006) 82.
[27] B. Brandt, T. Schalow, M. Laurin, S. Schauermann, J. Libuda, H.J. Freund, J. Phys. Chem. C 938 (2007) 111.
[28] H.J. Freund, Catal. Today 6 (2006) 117.
[29] C.R. Henry, C. Chapon, C. Duriez, J. Chem. Phys. 700 (1991) 95.
[30] K. Judai, S. Abbet, A.S. Wörz, M.A. Röttgen, U. Heiz, Int. J. Mass Spectrom. 99 (2003) 229.
[31] M.A. Röttgen, S. Abbet, K. Judai, J.M. Antonietti, A.S. Worz, M. Arenz, C.R. Henry, U. Heiz, J. Am. Chem. Soc. 9635 (2007) 129.
[32] M. Boudart, M.A. Vannice, J.E. Benson, Z. Phys. Chem. Frankfurt 171 (1969) 64.
[33] V. Matolin, E. Gillet, Surf. Sci. L 115 (1986) 166.
[34] L.N. Kantorovich, M.J. Gillan, Surf. Sci. 373 (1997) 374.
[35] U. Heiz, F. Vanolli, L. Trento, W.-D. Schneider, Rev. Sci. Instrum. 1986 (1997) 68.
[36] C. Di Valentin, A. Del Vitto, G. Pacchioni, S. Abbet, A.S. Wörz, K. Judai, U. Heiz, J. Phys. Chem. B 11961 (2002) 106.
[37] U. Heiz, J. Xu, J.T. Yates, J. Chem. Phys. 3925 (1994) 100.